Unimolecular Chemistry of Protonated Diols in the Gas Phase: Internal Cyclization and Hydride Ion Transfer

G. Bouchoux,*,† N. Choret,† and R. Flammang‡

Département de Chimie, Laboratoire des Mécanismes Réactionnels, URA CNRS 1307, Ecole Polytechnique, 91128 Palaiseau cedex, France, and Laboratoire de Chimie Organique, Université de Mons-Hainaut, 20 Place du Parc, B-7000 Mons, Belgium

Received: February 6, 1997; In Final Form: April 1, 1997[⊗]

Unimolecular dehydration of protonated α,ω-diols in the gas phase has been examined by both tandem mass spectrometry experiments, including metastable ions decompositions, collisional activation, and neutralization−reionization techniques, and molecular orbital calculations up to the MP2/6-311G**//MP2/6-31G*+ZPE level. Two reaction mechanisms were found to explain the experimental observations: one leading to a protonated cyclic ether via an internal nucleophilic substitution and one giving a protonated carbonyl species after hydride ion transfer from the α-carbon to the ω-position. Our major findings are the following: (i) protonated 1,2-ethanediol exclusively leads to protonated acetaldehyde via a concerted pinacol rearrangement with the calculated critical energy equaling 99 kJ/mol; (ii) protonated 1,3-propanediol gives protonated oxetane at low internal energy and protonated propanal at high internal energy with the calculated critical energies of the reactions equaling 144 and 163 kJ/mol, respectively, and the competition between the two reactions being explained by the internal energy effect upon dissociation rate constants; (iii) for 1,4-butanediol and 1,5-pentanediol, the dehydration produces only the corresponding protonated cyclic ether with calculated critical energies equal to 110 and 107 kJ/mol, respectively.

Introduction

In the gas phase[1] as well as in the condensed phase,[2] the chemistry of protonated diols is dominated by a dehydration process. In the latter case, it is well-established that the reaction of 1,4- and 1,5-diols, under various catalytic conditions, leads to the corresponding cyclic ether for which that reaction constitutes the most general preparative route. In contrast, 1,2- and 1,3-diols may give rise to more complicated behavior due, inter alia, to possible carbonium ion rearrangements. Dehydration of 1,2-diols in the solution phase leads to the classical pinacol rearrangement; the formation of epoxides from tetrasubstituted or hindered diols has been also reported. Generally the dehydration of 1,3-diols occurs in solution under acidic conditions to form the corresponding carbonyl compounds; oxetane is not usually produced.

Despite numerous mass spectrometric investigations of diols under chemical ionization conditions, the detailed mechanisms of the water loss from gaseous protonated diols is not fully rationalized. We choose to examine a series of protonated α,ω-diols in order to see if tendencies comparable to those in solution phase exist during the dehydration process of gaseous protonated diols. By analogy with solution phase chemistry, there are a priori two ways to model the dehydration of a protonated α,ω-diol in the gas phase, one leading to a protonated cyclic ether (path a, Scheme 1) and one giving a carbonyl protonated species (path b, Scheme 1).

The first process is an internal nucleophilic substitution reaction; the second involves an hydride ion transfer from the α-carbon to the ω-position. From a simple consideration of the enthalpy change associated with the two reactions, it may be expected that, when the number of carbon atoms separating the two hydroxyl groups increases, path a should be preferred to path b (Table 1). However, for both processes, the detailed mechanistic scheme, the critical energy needed by each reaction step, and the experimental details upon the water loss from an homologous series of diols are lacking or incomplete.

SCHEME 1

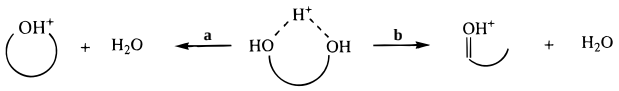

In the present study, we examine, both experimentally and theoretically, the four simplest alkanediols: 1,2-ethanediol, **1**; 1,3-propanediol, **2**; 1,4-butanediol, **3**; and 1,5-pentanediol, **4**. Tandem mass spectrometry experiments, and particularly multiple collisions processes,[4] have been undertaken to characterize the structure of the dehydration products. From a theoretical point of view, ab initio molecular orbital calculations including electron correlation effects have been done in order to model each reaction path.

Experimental and Computational Section

The reactions of metastable protonated diols were studied with a VG-ZAB-2F double focusing mass spectrometer (B-E) operating in the chemical ionization mode using methanol as reagent gas. The accelerating voltage was set at 8 kV, the electron energy at 150 eV, and the emission current at 0.5 mA. The source temperature was 180 °C. The mass analyzed ion kinetic energy (MIKE) spectra of metastable ions were obtained, as usual, by selecting with the magnet the ion to be studied and scanning the electrostatic analyzer voltage. The kinetic energy release distribution has been derived from the analysis of the metastable peak profile using the method described in ref 5.

The multiple collisional experiments were carried out with a VG-Analytical Auto Spec-6F mass spectrometer ($E_1B_1E_2$-$E_3B_2E_4$)[6] operating in the chemical ionization mode using methanol as reagent gas. The accelerating voltage was set at 8

† URA CNRS 1307.
‡ Université de Mons-Hainaut.
[⊗] Abstract published in *Advance ACS Abstracts,* May 15, 1997.

S1089-5639(97)00479-9 CCC: $14.00

TABLE 1: Thermochemical Data Relevant to the Gas Phase Dehydration of Protonated Diols 1−4 (kJ mol^{-1})

species	$\Delta_f H°_{298}$[a]	$\Delta_a H°_{298}$[b]	$\Delta_b H°_{298}$[b]
[1,2-ethanediol]H^+, **1H**$^+$	315[c]		
[oxirane]$H^+ + H_2O$	448	133	
[acetaldehyde]$H^+ + H_2O$	340		25
[1,3-propanediol]H^+, **2H**$^+$	242[d]		
[oxetane]$H^+ + H_2O$	382	140	
[propanal]$H^+ + H_2O$	307		65
[1,4-butanediol]H^+, **3H**$^+$	190[e]		
[tetrahydrofuran]$H^+ + H_2O$	265	75	
[butanal]$H^+ + H_2O$	278		88
[1,5-pentanediol]H^+, **4H**$^+$	150[f]		
[tetrahydropyran]$H^+ + H_2O$	223	73	
[pentanal]$H^+ + H_2O$	250		100

[a] From ref 3a, except for [tetrahydrofuran]H^+ and [tetrahydropyran]H^+ for which $\Delta_f H°_{298}$ are re-evaluated to conform to the new proton affinities of reference bases in ref 3b. [b] $\Delta_a H°_{298}$ and $\Delta_b H°_{298}$ represent the enthalpy variations of reactions a and b, Scheme 1. [c] From $\Delta_f H°_{298}$(**1**) = −388 kJ mol^{-1} (ref 3) and PA(**1**) = 827 kJ mol^{-1} (ref 1c). [d] From $\Delta_f H°_{298}$(**2**) = −408 kJ mol^{-1} and PA(**2**) = 880 kJ mol^{-1} (ref 1c). The tabulated $\Delta_f H°_{298}$(**2**) value[3] (−392 kJ mol^{-1}) appears to be too high. When considering the $\Delta_f H°_{298}$ values calculated by the Benson's incremental method (−385, −406, −426, −447 for 1−4, respectively), an excellent agreement, within 3 kJ mol^{-1}, is observed with the data of ref 3a, except for 1,3-propanediol, **2**, for which the difference attains 14 kJ mol^{-1}. We thus choose to homogenize the heat of formation of gaseous diols by assigning $\Delta_f H°_{298}$(**2**) = −408 kJ mol^{-1}. [e] From $\Delta_f H°_{298}$(**3**) = −427 kJ mol^{-1} (ref 3) and PA(**3**) = 913 kJ mol^{-1} (ref 1c). [f] From $\Delta_f H°_{298}$(**4**) = −449 kJ mol^{-1} (ref 3) and PA(**4**) = (930 kJ mol^{-1}). The latter has been deduced from PA(**3**) and the calculated heat of isodesmic reaction, **3H**$^+$ + **4** → **4H**$^+$ + **3**.

kV, the electron energy at 70 eV, and the emission current at 1 mA. The source and the septum inlet temperatures were 200 and 160 °C respectively. For the experiments denoted CA-He, the ions of interest were selected by E_1B_1 and subjected to collisional activation (CA) with helium in the third field free region (FFR) of the instrument; the helium pressure was adjusted in order to reduce the signal to ca. 70% of its original value. The fragments were then analyzed by scanning E_2 and detected by the off-axis photomultiplier located in the fourth FFR. The CA (O_2) spectra were obtained in a similar way by selection of the ions with $E_1B_1E_2$ and collisional activation with dioxygen in a gas cell located in the fourth FFR; the fragments were analyzed with E_3 and detected by the off-axis photomultiplier located in the fifth FFR. During the MS/MS/MS experiments, the ions produced in the third FFR by dissociation of a precursor selected by E_1B_1 are further selected by E_2 and subjected to collisional activation with O_2 in the gas cell situated before E_3; the fragments are analyzed by scanning E_3. The neutralization−reionization (NR) experiments are performed by successive collisions with ammonia and dioxygen in the two gas cells situated in the fourth FFR. Species non-neutralized in the first cell are deflected by an intermediate electrode raised at a potential of 9 kV.

The experimental data are collected in Tables 2, 4, 6, and 8 and Figures 1, 5, 9, and 12; the CA (He) and CA (O_2) spectra are the result of 30 signal accumulations (corresponding to an acquisition time of 45 s), and NR spectra are the average of 100 scans (acquisition time = 150 s). The chemical samples (diols, aldehydes, and oxacycloalkanes) are commercial compounds (Aldrich Chemical) of research grade; high-purity gases were used in the collision experiments: helium 5.0, oxygen 2.6, ammonia N45 (Praxair).

All ab initio molecular orbital calculations were performed using a local version of the GAUSSIAN 94 set of programs.[7] Stationary points have initially been located by geometry optimization using single-reference Hartree−Fock (HF) wave functions with the polarized 6-31G* basis set. Depending upon the size of the system, geometrical parameters of relevant structures have then been reoptimized at the second-order Möller−Plesset perturbation (MP2/6-31G*) level. Stable structures and saddle points were characterized by harmonic vibrational analysis at these levels. Zero-point vibrationnal energies, ZPE, are estimated from HF/6-31G* (MP2/6-31G*) vibrational wavenumbers and scaled by 0.9 (0.97). Improved relative energies have subsequently been obtained from single-point total energy calculations with the larger 6-311G** basis sets. The calculated total and relative energies are summarized in Tables 3, 5, 7, and 9.

Results and Discussion

Protonated 1,2-Ethanediol, 1H$^+$. 1,2-ethanediol is known to give an abundant [**1H**−H_2O]$^+$ ion under chemical ionization conditions.[1] This ion is also responsible for the exclusive signal in the MIKE spectrum of **1H**$^+$, moreover, H/D exchange in the ion source demonstrates that water loss concerns exclusively the hydroxylic and the protonating hydrogens. The metastable dissociation **1H**$^+$ → [**1H**−H_2O]$^+$ is associated with a simple Gaussian peak, in keeping with a single reaction path. The following kinetic energy release values were deduced from the analysis of the metastable peak profile: $T_{0.5}$ = 37 ± 4 meV and $T_{average}$ = 105 ± 10 meV.

The characterization of the [**1H**−H_2O]$^+$ ions may be done by tandem mass spectrometry experiments. Collisional activation (CA) spectra of various $[C_2H_5O]^+$ ions have been previously reported.[8] Chen and Stone[1c] showed that the CA spectrum of [**1H**−H_2O]$^+$ and protonated acetaldehyde are comparable, but they did not examine protonated oxirane. The results obtained on the six-sectors instrument of the Mons University using either helium or dioxygen as the collision gas are presented in Table 2.

The CA(He) mass spectrum of [**1H**−H_2O]$^+$ is characterized by a dominant loss of methane (which is also the unimolecular dissociation). As shown in Table 2 this spectrum is not very different from those of protonated acetaldehyde (with which the closest resemblance is noted) or protonated oxirane. On the latter spectrum and as already observed,[8] one may note more intense signals at *m/z* 19 and *m/z* 31 and a less intense peak at *m/z* 15. The differences between the CA spectra are not significantly more pronounced when dioxygen is used as the collision gas.[4f] In addition to the preceding observations, a loss of 15 u becomes important, and the corresponding signal constitutes the base peak in the spectrum of protonated acetaldehyde. From these observations, it seems hard to

TABLE 2: CA (He) and CA (O_2) Spectra of *m/z* 45 Ions Generated by Chemical Ionization from 1,2-Ethanediol (1), Acetaldehyde (1a), and Oxirane (1b)

		44	43	42	41	40	31	30	29	28	27	26	25	24	19	18	17	16	15	14	13	12
He	**1**	16	31	8	<1		<1	7	100	8	68	44	6	<1	3		<1	<1	29	9	<1	
	1a	30	30	12	<1		<1	10	100	12	72	51	9	<1	2		<1	<1	35	12	1	
	1b	12	42	8			5	8	100	10	78	45	8		12				21	9		
O_2	**1**	45	116	43	7	<1	8	78	100	20	47	32	8	1	6			1	17	7	1	
	1a	71	96	39	8	1	12	126	100	27	47	37	10	3	5	1	1	2	24	11	3	1
	1b	23	109	35	6	<1	13	53	100	17	57	31	8	2	15			1	14	7	1	

TABLE 3: Total (hartree) and Relative (kJ mol^{-1}) Energies Calculated for the Protonated 1,2-Ethanediol System

	MP2(FC)/6-31G*		MP2(full)/6-31G*			MP2(FC)/6-311G** // MP2(full)/6-31G*		
species	total	rel	total	rel	ZPE[a]	total	rel	+ZPE
1H$_a$ $^+$	−229.859 51	0	−229.874 29	0	241	−230.036 99	0	0
1C$_1$ (trans)	−229.837 96	57	−229.852 65	57	239	−230.017 23	52	50
1TS−C	−229.817 78	110	−229.832 19	111	231	−229.994 27	112	102
1C$_2$	−229.825 32	90	−229.839 78	91	231	−230.003 16	89	79
[oxirane]H$^+$	−153.604 59		−153.616 50		174	−153.712 07		
H_2O	−76.196 85		−76.199 24		52	−76.267 61		
[oxirane]H$^+$ + H_2O	−229.801 44	153	−229.815 74	154	226	−229.979 68	150	135
1C′$_2$	−229.851 49	21	−229.866 13	21	232	−230.029 80	19	10
1TS−H	−229.810 40	129	−229.825 05	129	223	−229.992 56	117	99
[acetaldehyde]H$^+$	−153.644 86		−153.656 92		169	−153.754 52		
[acetaldehyde]H$^+$ + H_2O	−229.841 71	47	−229.856 16	48	220	−230.022 13	39	18
1C$_4$	−229.892 36	−86	−229.907 07	−86	227	−230.072 83	−94	−108
1TSC$_2$/C$_4$			−229.805 43	181	218	−229.971 75	171	148

[a] ZPE (corrected by the factor 0.97) in kJ mol^{-1}.

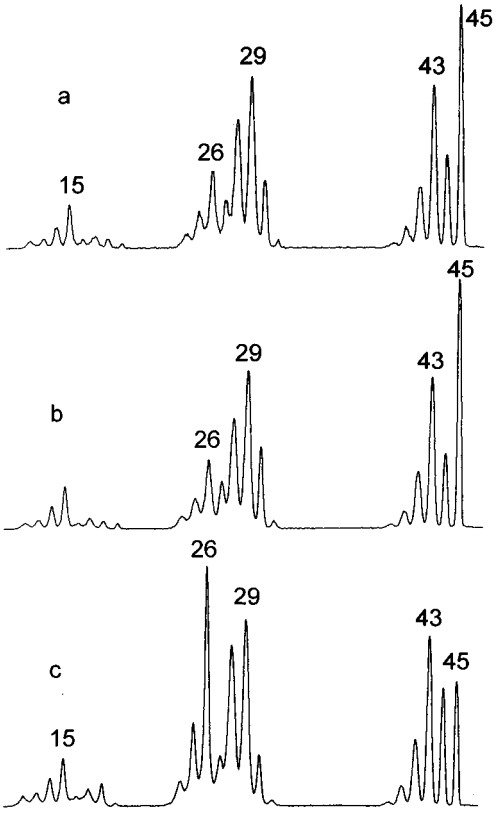

Figure 1. NR (NH_3/O_2) mass spectra of $[C_2H_5O]^+$ ions (*m/z* 45) produced from 1,2-ethanediol (**1**) (a), acetaldehyde (**1a**) (b), and oxirane (**1b**) (c).

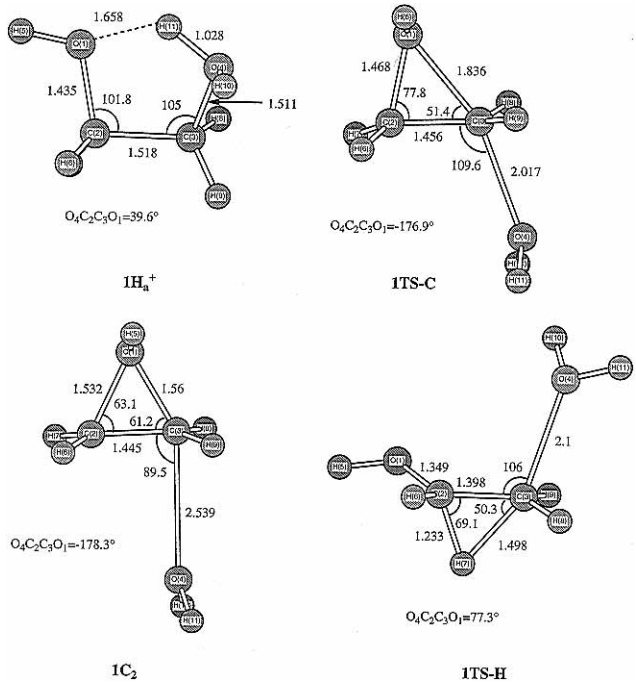

Figure 2. Geometrical parameters of some structures relevant to the protonated 1,2-ethanediol system. Bond lengths are reported in angstroms and bond angles in degrees (MP2(full)/6-31G* optimized geometries).

unambiguously decide if the $[\mathbf{1H}-H_2O]^+$ ion structure is protonated acetaldehyde alone or in a mixture with protonated oxirane.

A more efficient way to distinguish between these *m/z* 45 ion structures is offered by their neutralization−reionization spectra. As shown in Figure 1, identical spectra are obtained for $[\mathbf{1H}-H_2O]^+$ and protonated acetaldehyde. Important differences are observed on the NR spectrum of protonated oxirane: less abundant recovered signal and larger intensities for the peaks at *m/z* 18 and 26.

The neutralization of $[CH_3CHOH]^+$ ion is expected to give rise to a stable radical. This is confirmed by the high intensity of the recovered signal and by a NR spectrum comparable to the CA (O_2) spectrum (Table 2) in that case. This indicates that the $[CH_3CHOH]^\bullet$ radical has a lifetime greater than the delay of ca. 1 μs necessary to travel the distance between the neutralization and the reionization cells. In contrast, the neutralization of protonated oxirane would lead to an unstable hypervalent radical which probably regenerates neutral oxirane. The observations of peaks at *m/z* 18 and 26 in the NR mass spectrum and of *m/z* 19 in the CA (He, O_2) mass spectra of protonated oxirane may be interpreted by the parallel formation of a proton bound complex $C_2H_2\cdots H_3O^+$ during the protonation process.[8d] The exact matching of the NR spectra of $[\mathbf{1H}-H_2O]^+$ ions and of protonated acetaldehyde, particularly in the *m/z* 24−32 region, demonstrates that the dehydration of $\mathbf{1H}^+$ leads exclusively to $[CH_3CHOH]^+$ ions in the source of the mass spectrometer.

In summary, the experimental informations indicate that the dehydration of protonated 1,2-ethanediol occurs via a single mechanism at low internal energy and that the source-produced $[\mathbf{1H}-H_2O]^+$ ion is protonated acetaldehyde.

The results of the molecular orbital calculations conducted on this system are summarized in Table 3.

The most stable conformation of protonated 1,2-ethanediol, **1H$_a$**$^+$, corresponds to a dihedral angle OCCO of 39.6° at the MP2(full)/6-31G* level (Figure 2). This result is in reasonable agreement with that obtained previously at the MP2/6-31G*//

SCHEME 2

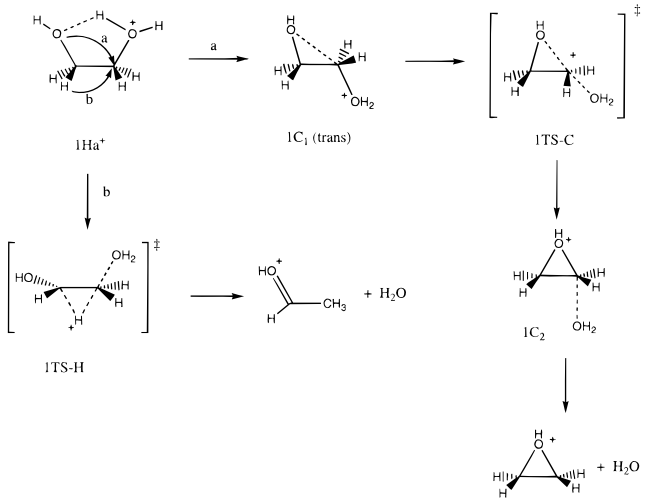

3-21G level[9] (OCCO = 45°). The structure $\mathbf{1H_a}^+$ allows an internal hydrogen bond length of 1.66 Å, a value larger by ca. 0.44 Å than that we have calculated (MP2(FC)/6-31G*) for the proton-bonded complex between protonated and neutral methanol:

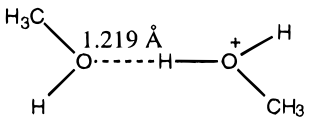

This situation reflects the unfavored dipole−dipole interactions and steric constraints which limit the extent of the internal hydrogen bond in $\mathbf{1H_a}^+$. Another proof is given by the limited stabilization energy of this conformation which may be illustrated by the fact that the anti conformation, for which the OCCO angle is equal to 180°, lies only 50 kJ/mol above $\mathbf{1H_a}^+$ (MP2(FC)/6-311G**//MP2(full)/6-31G* calculation, Table 3), an energy markedly smaller than the bimolecular H-bond energy calculated (MP2(FC)/6-31G*+ZPE) for the system $CH_3OH_2^+ + CH_3OH$ (151 kJ/mol). The various steps involved during the two possible dehydration reactions of $\mathbf{1H}^+$ are depicted in Scheme 2.

Experimentaly, the two reactions are associated with endothermicities $\Delta_a H°_{298}$ and $\Delta_b H°_{298}$ of 133 and 25 kJ/mol (Table 1), in good agreement with the calculated 298 K values of 140 and 26 kJ/mol.

In order to create a new C−O bond starting from $\mathbf{1H_a}^+$ during the cyclodehydration reaction, it is first necessary to rotate the molecule around the C(2)−C(3) bond to attain the $\mathbf{1H}^+$ trans conformation (structure $\mathbf{1C_1}$, Scheme 2). This conformational change has been studied elsewhere, and the transition structure was predicted to lie 65 kJ/mol above $\mathbf{1H_a}^+$ and only 5 kJ/mol above the OCCO = 180° conformation (MP2/6-31G*//3-21G calculations).[9] It may be noted that the trans conformer $\mathbf{1C_1}$ is a species slightly stabilized by a favorable interaction between O(1) and C(3) as attested by the O(1)C(2)C(3) angle value of 100° and by the small increase of the C(3)O(4) bond length (1.53 Å). The gas phase hydrolysis of protonated oxirane, which is the reverse of the cyclodehydration reaction, was studied theoreticaly in 1987 by Ford and Smith.[10] Our results, obtained at a higher level of theory, confirm some of their conclusions. Starting from the trans conformer $\mathbf{1C_1}$, the shortening of the O(1)···C(3) distance is a continuously endothermic process until the transition structure **1TS−C** is attained. Then, there is formation of an ion-neutral complex $\mathbf{1C_2}$ which further dissociates into protonated oxirane plus H_2O. The stabilization energy of complex $\mathbf{1C_2}$, with respect to protonated oxirane plus H_2O, is equal to 56 kJ/mol. The energy-determining step of the overall cyclodehydration reaction is the dissociation of the ion-neutral complex $\mathbf{1C_2}$ into its components.

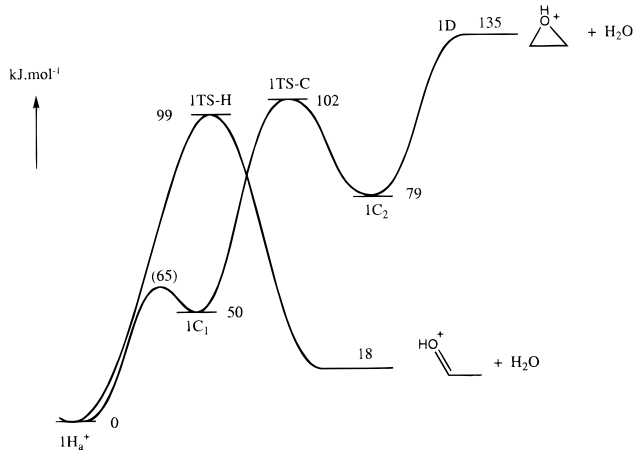

Figure 3. Schematic potential energy profile for dehydration reactions from the protonated 1,2-ethanediol system (MP2/6-311G**//MP2/6-31G*+ZPE calculations and (in parentheses) MP2/6-31G*//HF/3-21G calculations of ref 12).

The second dehydration reaction of $\mathbf{1H}^+$ involves a 1,2-hydride ion shift concerted with the departure of the water molecule (the prototype of the "pinacol" rearrangement, reaction b, Scheme 2). The present data confirm the conclusions of Nakamura and Osamura[11] who showed that this process is a concerted reaction rather than a stepwise elimination involving transient β-hydroxycarbenium cation, $[CH_2CH_2OH]^+$. In fact, the latter isolated species is not a stable structure and collapses readily to the α-hydroxycarbenium ion $[CH_3CHOH]^+$; in the present system this structural change is concerted with the water elimination. The transition structure of this concerted reaction, **1TS−H**, is situated 99 kJ/mol above $\mathbf{1H_a}^+$. We note that this calculated value is in perfect agreement with previous computations[11] but markedly higher than the estimate of 56 kJ/mol based on a kinetic treatment of experimental data obtained by high-pressure mass spectrometry.[1c]

It appears, from examination of Figure 3, that the dehydration route leading to protonated acetaldehyde (reaction b, Scheme 2) is favored, by 36 kJ/mol (energy difference between protonated oxirane plus H_2O and **1TS−H**), over the cyclodehydration process (reaction a, Scheme 2).

However, the rate-determining step of the two reactions are in essence different. In the former case, it is a concerted 1,2-hydride ion shift/water elimination process. For the latter reaction it is only the separation of the two components of the loosely bound complex $\mathbf{1C_2}$. Consequently it may be expected that the competition will favor reaction **a** at high energy. The fact, established by the experimental data, that this is apparently not the case may be briefly discussed. To elucidate this question, calculations of the unimolecular rate constants associated with the two possible dehydration reactions giving protonated acetaldehyde (reaction b, Scheme 2), k_{1b}, and protonated oxirane (reaction a, Scheme 2), k_{1a}, have been undertaken. The Rice−Ramsperger−Kassel−Marcus (RRKM) formulation[13] of the rate constant has been used in conjunction with the Stein−Rabinovitch algorithm[14] to evaluate the sums and densities of vibrational states. The rate constant for reaction b is simply given by

$$k_{1b} = k_H = \sum P^{\ddagger}_{1TS-H}(E - E_{01})/hN_{1H}(E)$$

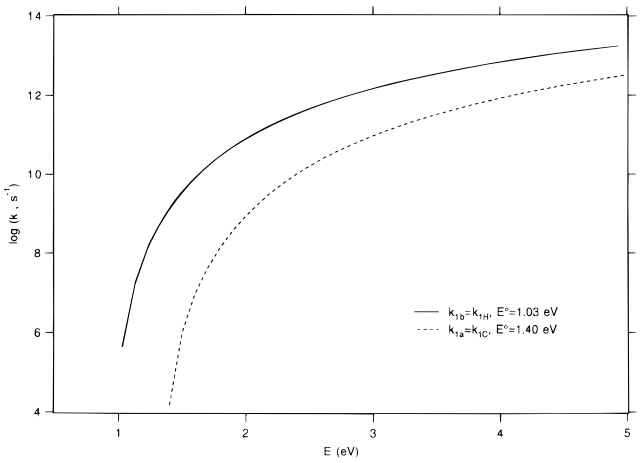

Figure 4. RRKM rate constants for the pinacolic rearrangement (k_{1H}) and the cyclodehydration (k_{1C}) reaction from protonated 1,2-ethanediol.

where $\sum P^{\ddagger}_{\mathbf{1TS-H}}(E - E_{01})$ represents the sum of vibrational states of the transition structure **1TS−H** containing the excess energy $E - E_{01}$ and $N_{\mathbf{1H}}(E)$ the density of vibrational states of the parent ion $\mathbf{1H_a}^+$ of internal energy E. Reaction **a** is a multistep process for which three elementary rate constants may be defined, if we neglect the incidence of the passage though **1C₁**:

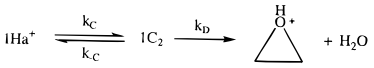

By using the steady state approximation to the transient species **1C₂** and the inequalities $k_D < k_{-C}$ and $k_C \ll k_D$ resulting from the corresponding critical energy values (Figure 3), the overall rate constant for reaction a, k_{1a}, may be approximated by

$$k_{1a} = \sum P^{\ddagger}_{\mathbf{1D}}(E - E_{03})/hN_{\mathbf{1H}}(E)$$

where **1D** refers to the loose transition state associated with dissociation of **1C₂**.

The sums, $\sum P^{\ddagger}_{\mathbf{i}}(E - E_0)$ and the densities, $N_{\mathbf{1H}}(E)$, of the vibrational states have been evaluated from the calculated MP2/6-31G* frequencies scaled by 0.97 (internal rotations were treated in the harmonic vibrator approximation) and using the critical energies $E_{01} = 99$ kJ/mol (1.03 eV) and $E_{03} = 135$ kJ/mol (1.40 eV) calculated at the MP2/6-311G**//MP2/6-31G*+ZPE level. The loose transition structure **1D** has not been successfully located because of the flatness of the potential energy surface in this region. Consequently, the corresponding vibrational frequencies have been calculated for a **1C₂** species characterized by a fixed C(3)O(4) distance of 3.0 Å, all the other geometrical parameters being optimized. The internal energy dependence of the two corresponding rate constants is presented in Figure 4.

The observation that k_{1b} is always greater than k_{1a} by 1−5 orders of magnitude confirms that only the concerted reaction b (Scheme 2) is occurring at the all-energy regime and that no protonated oxirane may be formed from $\mathbf{1H}^+$ at low, as well as at high, internal energy.

SCHEME 3

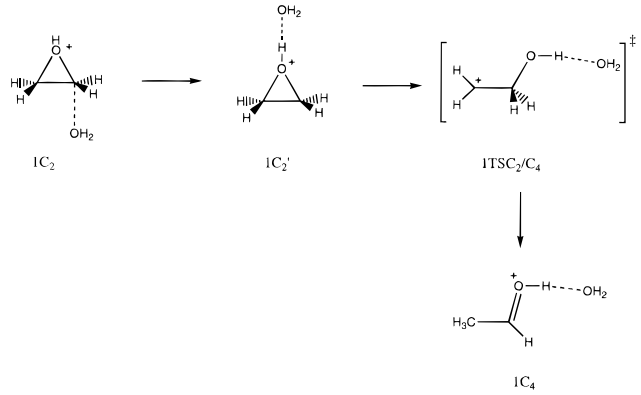

A second observation that emerges from examination of Figure 3 is that the critical configuration **1TS−C** involved in the first step of reaction **a** is virtually at the same energy level as **1TS−H**. It is thus highly probable that, besides protonated acetaldehyde, some **1C₂** complexes are competitively produced. Furthermore this latter may be at the origin of a second way of formation of protonated acetaldehyde inside ion-neutral complexes as indicated in Scheme 3.

It is known[10,12] that isolated protonated oxirane may interconvert to protonated acetaldehyde via an appreciable energy barrier (116 kJ/mol, MP2/6-31G* calculations[12b]). We investigate the analogous water-solvated reaction **1C′₂** → **1C₄** in order to see whether the complex-mediated reaction sketched in Scheme 3 is a plausible mechanism for the formation of protonated acetaldehyde. Our calculations show that the two complexes **1C′₂** and **1C₄** are identically stabilized by ca. 125 kJ/mol (Table 3). Secondly, the transition structure **1TS−C₂/C₄** is calculated to lie 148 kJ/mol above $\mathbf{1H_a}^+$, i.e. 130 kJ/mol above the products $[CH_3CHOH]^+ + OH_2$. One should observe that the critical energy for the water-solvated isomerization **1C′₂** → **1C₄** (138 kJ/mol) is higher than that of the isolated reaction (116 kJ/mol[12b]). This difference is accounted for by the nature of the interaction between the water molecule and the bounded hydrogen in the couple reactants/products and in the transition structure. It has been noted above that **1C′₂** and **1C₄** possess the same stabilization energies, this is in keeping with comparable $H_2O\cdots H$ distances (1.457 and 1.446 Å, respectively) and identical net charges on the hydrogen atom (0.61). In contrast, for the transition structure **1TS−C₂/C₄** the $H_2O\cdots H$ is lengthened to 1.69 Å because most of the positive charge of the cation is supported by the CH_2 moiety thus inducing a lowering of the positive charge on the hydrogen atom (0.56) and consequently a lowering of the hydrogen bonding.

The transition structure **1TS−C₂/C₄**, which constitutes with high probability the rate-determining step in the overall process of Scheme 3, is too high in energy to efficiently compete with the concerted pinacol rearrangement which is predicted to need only 99 kJ/mol (**1TS−H**). It appears consequently that the route

TABLE 4: CA (He) and CA (O_2) Spectra of *m/z* 59, $[C_3H_7O]^+$ Ions, Generated by Chemical Ionization from 1,3-Propanediol (2), Propanal (2a), and Oxetane (2b)

		58	57	56	55	53	44	43	42	41	40	39	38	37	31	30	29	28	27	26	15
He	**2**	2	10					6	2	105	1	28	3	<1	220	7	100	26	64	20	
	2a	6	8					10	3	40		26	3	<1	109	7	100	31	65	18	
	2b		27					5	1	104	5	36	10	4	381	22	100	60	75	43	
O_2	**2**	31	72		9	1	17	40	23	113	15	46	15	9	231	36	100	54	57	28	
	2a	85	106	5	13	2	29	48	33	68	15	51	14	8	133	38	100	49	54	26	<1
	2b	13	105		7		3	18	8	186	17	37	12	5	585	38	100	70	55	27	

depicted in Scheme 3 could not be efficient and that the unique way to generate protonated acetaldehyde by dehydration of protonated 1,2-ethanediol is the concerted process involving the transition structure **1TS−H** (reaction **b**, Scheme 2). This conclusion confirms the deductions based on experiments which demonstrate the dominant formation of protonated acetaldehyde and occurrence of a single reaction mechanism in the metastable time frame.

Protonated 1,3-Propanediol, $2H^+$. Among the four compounds **1**−**4** studied here, 1,3-propanediol gives the less abundant $[MH\text{-}H_2O]^+$ ions under chemical ionization conditions; the abundances ratio $[\mathbf{2H}-H_2O]^+/\mathbf{2H}^+$ is only equal to 0.05 using methane as reagent gas.[1c] Water loss is the exclusive fragmentation of metastable $\mathbf{2H}^+$ ions, and this reaction involves only the protonating and the hydroxylic hydrogens. The signal in the MIKE spectrum is simple Gaussian, and the following kinetic energy release values may be deduced from the analysis of the metastable peak profile: $T_{0.5} = 21 \pm 2$ meV and $T_{average} = 56 \pm 7$ meV. Identification of $[C_3H_7O]^+$ ions produced by dehydration of $\mathbf{2H}^+$ occurring either in the source or in the third field free region of the mass spectrometer has been attempted by collisional experiments. It has been reported a long time ago,[16] and recently confirmed,[17] that protonation of oxetane gives $[C_3H_7O]^+$ ions whose CA spectrum is very similar to that of protonated propionaldehyde.

Our results (Table 4) are in line with these observations. Excluding the two signals at *m/z* 41 and 31, which correspond also to unimolecular dissociations, the CA (He) of protonated propanal and oxetane show clear similarities but also small differences. In particular, for the latter ions, more pronounced signals appear at *m/z* 57, 30, 28, and 26 and an unresolved peak at *m/z* 38−39 should be noted. The CA (He) spectrum of the source-produced $[\mathbf{2H}-H_2O]^+$ ions present slightly better analogies with that of protonated propanal. More firm conclusions may be drawn from the CA (O_2) spectra. The two reference structures are distinguishable by comparison of the *m/z* 37−45 region and the *m/z* 58 signal (Table 4), and it appears more clearly that the spectrum of the source-produced $[\mathbf{2H}-H_2O]^+$ ions is closer to that of protonated propanal; however, these comparisons do not exclude the possibility of a mixture of protonated propanal and protonated oxetane.

Finally, the NR spectra allow another means to differenciate both protonated propanal and protonated oxetane (Figure 5A).

The former leads to an intense recovered signal in agreement with the formation of a stable $CH_3CH_2C^{\bullet}HOH$ radical; the signals in the range *m/z* 37−44 are specific of this structure. In the case of protonated oxetane, no significant recovered signal is observed, and interestingly enough, the major fragment corresponds to ionized ethene. As seen in Figure 5A, a clear analogy exists between the NR spectra of protonated propanal and that of $[\mathbf{2H}-H_2O]^+$ ions produced in the source of the mass spectrometer. However, a slight lowering in intensities of peaks *m/z* 59−57, *m/z* 44−37 and *m/z* 31−29 may be indicative of a parallel formation of protonated oxetane.

As pointed out in the introduction, formation of protonated propanal by dehydration of $[\mathbf{2H}-H_2O]^+$ ions is the less endothermic process (65 kJ/mol compared to 140 kJ/mol for the formation of protonated oxetane). The preceding theoretical study of 1,2-ethanediol revealed, however, that the route leading to protonated aldehyde may involve an important activation barrier, and this point will be fully confirmed here (see below). Thus it was of interest to examine more deeply the possibility of formation of protonated oxetane at low internal energy. For this purpose, MS/MS/MS experiments have been done in order to characterize $[C_3H_7O]^+$ ions produced in flight from metastable ions $[\mathbf{2H}]^+$. The CA (O_2) spectrum of $[C_3H_7O]^+$ ions generated by dissociation of $[\mathbf{2H}]^+$ in the third field free region of the six-sectors instrument (see Experimental and Computational Section) is presented in Figure 5B together with the CA (O_2) spectra of the reference structures obtained at identical collisional energy (6130 eV = laboratory frame kinetic energy). Figure 5B shows clearly identical spectra for $[\mathbf{2H}-H_2O]^+$ ions and

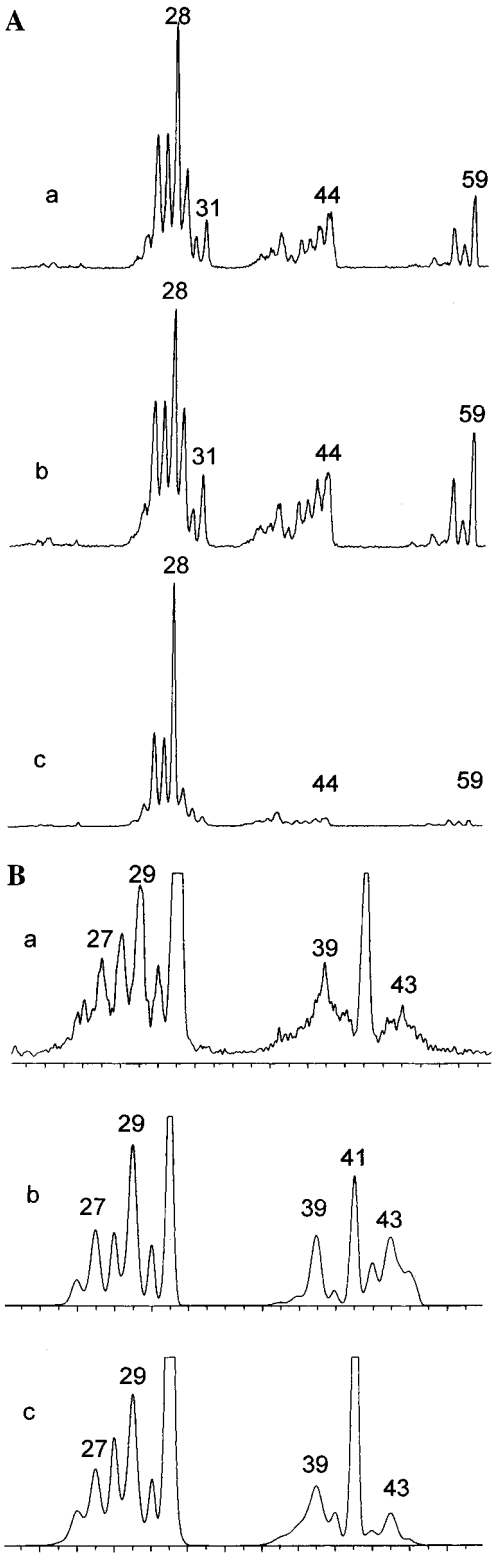

Figure 5. (A) NR (NH_3/O_2) mass spectra of $[C_3H_7O]^+$ ions (*m/z* 59) produced from 1,3-propanediol (**2**) (a), propanal (**2a**) (b), and oxetane (**2b**) (c). (B) Part of the CA (O_2) mass spectra of $[C_3H_7O]^+$ ions (*m/z* 59) produced during the flight from metastable $[\mathbf{2H}]^+$ ions (a), from protonated propanal (**2a**) (b), and from protonated oxetane (**2b**) (c).

TABLE 5: Total (hartree) and Relative (kJ mol^{-1}) Energies Calculated for the Protonated 1,3-Propanediol System

	HF/3-21G		HF/6-31G*		MP2(full)/6-31G*			MP2(FC)/6-311G**//MP2(full)/6-31G*		
species	total	rel	total	rel	total	rel	ZPE[a]	total	rel	+ZPE
2H$_b$ $^+$ (trans)					−269.030 13	98	312	−269.220 21	95	97
2H$_a$ $^+$	−266.855 05	0	−268.297 05	0	−269.067 31	0	310	−269.256 46	0	0
2C$_1$	−266.815 96	103	−268.275 85	56	−269.038 81	75	312	−269.228 30	74	76
2**TS**−**C**	−266.799 22	147	−268.256 14	107	−269.015 18	137	305	−269.202 42	142	137
2C$_2$	−266.803 89	134	−268.267 44	78	−269.030 05	98	305	−269.218 52	100	95
[oxetane]H$^+$	−191.190 59		−192.238 68		−192.809 75		248	−192.930 08		
H$_2$O	−75.585 96		−76.010 75		−76.199 24		52	−76.267 61		
[oxetane]H$^+$ + H$_2$O	−266.776 55	206	−268.249 43	125	−269.008 99	153	300	−269.197 69	154	144
2C$_3$	−266.835 94	50	−268.285 91	29	−269.053 87	35	307	−269.242 42	37	34
2**TS**−**H**	−266.729 55	330	−268.227 99	181	−268.993 81	193	294	−269.188 29	179	163
[propanal]H$^+$	−191.193 20		−192.265 79		−192.832 31		241	−192.955 42		
[propanal]H$^+$ + H$_2$O	−266.779 16	199	−268.276 54	54	−269.031 55	94	293	−269.223 03	88	71
2C$_5$	−266.847 76	19	−268.317 39	−53	−269.081 15	−36	300	−269.272 40	−42	−52

[a] ZPE (corrected by the factor 0.97) in kJ mol^{-1}.

SCHEME 4

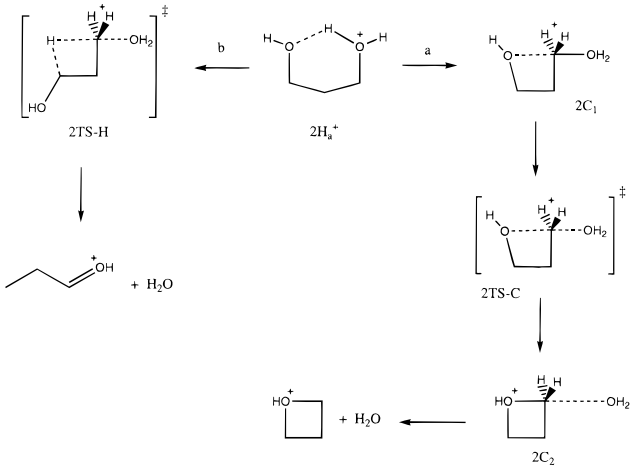

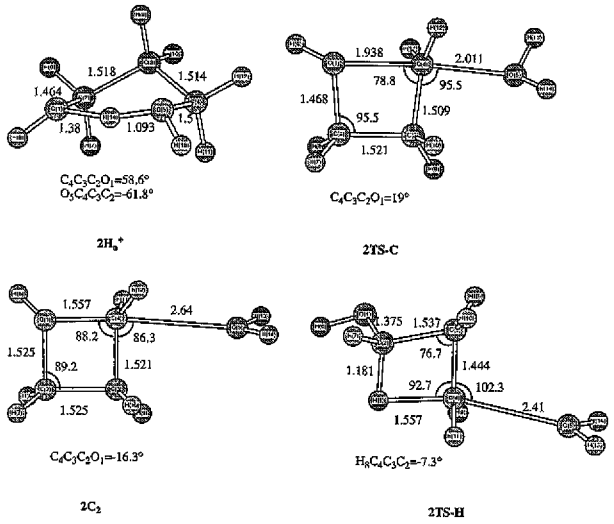

Figure 6. Geometrical parameters of some structures relevant to the protonated 1,3-propanediol system. Bond lengths are reported in angstroms and bond angles in degrees (MP2(full)/6-31G* optimized geometries).

protonated oxetane. It appears consequently that ions [**2H**]$^+$ of low internal energy generate preferentially protonated oxetane. The situation is in contrast to what has been observed at higher energy where the major, if not exclusive, dehydration product is protonated propanal. This contrasted behavior will be now examined in the light of molecular orbital calculations.

The two isomerization/dissociation routes investigated in order to model the dehydration processes of [**2H**]$^+$ are presented in Scheme 4. They involve cyclization by internal nucleophilic substitution (reaction a) and 1,3-hydride ion migration (reaction b).

The computational results are summarized in Table 5, and the geometry of some stationary points are presented in Figure 6.

A first observation concerns the accuracy of the computational data: a reasonable agreement is found between experimental reaction enthalpy, $\Delta_a H°_{298}$ = 140 kJ/mol and $\Delta_b H°_{298}$ = 65 kJ/mol (Table 1), and the corresponding calculated 298 K values of 149 and 78 kJ/mol.

The pseudo chair structure **2H$_a$**$^+$ (Figure 6) is the most stable conformation of [**2H**]$^+$ ions. As expected, the internal hydrogen bond is more efficient in **2H$_a$**$^+$ than in the lower homolog **1H$_a$**$^+$. This is reflected by the smaller H-bond length of 1.38 Å which approaches the value calculated for the bimolecular system CH_3-OH_2···$OHCH_3$ (1.219 Å). An estimate of the H-bond energy, including the strain energy effect, is provided by the energy difference between **2H$_a$**$^+$ and the all-trans conformation **2H$_b$**$^+$, i.e. 97 kJ/mol (Table 5).

The cyclodehydration reaction of **2H**$^+$ (reaction a, Scheme 4) follows a path comparable to **1H**$^+$. The first step is the formation of the structure **2C$_1$** (Scheme 4) in which an internal stabilization is provided by a favorable interaction between O(1) and C(4) (interatomic distance = 2.668 Å) and where the C(4)−O(5) bond begins its elongation (1.548 Å). The following step is the ring closure process leading to the formation of an ion-neutral complex **2C$_2$** for which a stabilization energy of 49 kJ/mol is calculated. The transition structure connecting **2C$_1$** to **2C$_2$**, **2TS**−**C**, has been located, and our best estimate of its relative energy is 137 kJ/mol (Figure 7). These events are followed by the dissociation of the complex **2C$_2$** into protonated oxetane plus H_2O by a continuously endothermic process. The dissociation of the ion-neutral complex **2C$_2$** into its components constitutes in fact the energy-determining step of the overall cyclodehydration reaction (**2D**, Figure 7).

The concerted dehydration pathway associated with a 1,3-hydride ion migration (reaction b, Scheme 4) involves a transition structure **2TS**−**H** situated 163 kJ/mol above **2H$_a$**$^+$ and 92 kJ/mol above the dissociation products, protonated propanal and water. Moreover, structure **2TS**−**H** is 19 kJ/mol above the cyclodehydration products: protonated oxetane and water.

The general potential energy profile associated with reactions a and b (Figure 7) seems to parallel the experimental observation of the favored formation of protonated oxetane at low internal energy. However, to explain the competitive formation of protonated propanal at high internal energy the overal rate

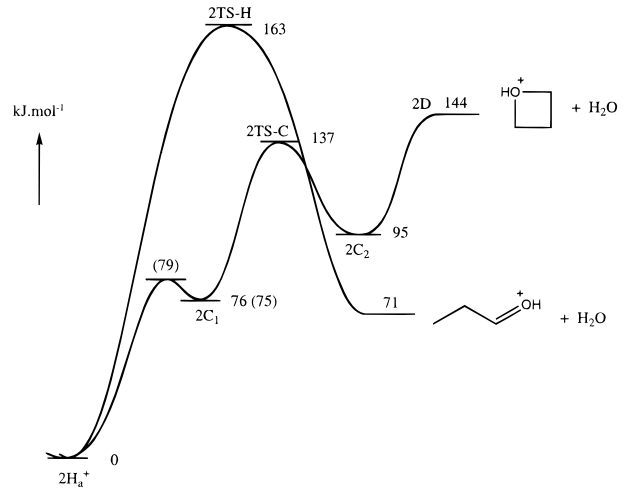

Figure 7. Schematic potential energy profile for dehydration reactions from the protonated 1,3-propanediol system (MP2/6-311G**//MP2/6-31G*+ZPE and (in parentheses) MP2/6-31G*//MP2/6-31G* calculations).

constant of reaction a must increase more rapidly with energy than that of reaction b. In order to check this expectation, the calculation of the two rate constants k_a and k_b corresponding to reactions a and b has been done using the RRKM theory. For reaction b the rate constant is simply given by

$$k_{2b} = k_H = \sum P^{\ddagger}_{\mathbf{2H}}(E - E_{OH})/hN_{\mathbf{2}}(E)$$

where $\sum P^{\ddagger}_{\mathbf{2H}}(E - E_{OH})$ and $N_{\mathbf{2}}(E)$ concern the transition structure **2TS−H** and the parent ion $\mathbf{2H_a}^+$, respectively; the critical energy E_{0H} has been taken equal to 163 kJ/mol (1.69 eV).

In the case of reaction a, the situation is more complex as long as the stable intermediate $\mathbf{2C_2}$ is formed with a critical energy close to that of the dissociation. Neglecting the incidence of the intermediate $\mathbf{2C_1}$, three elementary rate constants, k_C, k_{-C}, and k_D, should be considered:

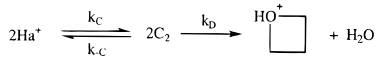

If one applies the steady state approximation to $\mathbf{2C_2}$ and assumes that $k_{-C} \approx k_D \gg k_C$, as expected in view of the corresponding critical energies, then the overal rate constant k_{2a} may be approximated[19] by

$$k_{2a} \approx [k_D/(k_D + k_{-C})]k_C$$

i.e.

$$k_{2a} \approx [\sum P^{\ddagger}_{\mathbf{2D}}(E - E_{0D})/(\sum P^{\ddagger}_{\mathbf{C}}(E - E_{0C}) + \sum P^{\ddagger}_{\mathbf{2D}}(E - E_{0D}))][\sum P^{\ddagger}_{\mathbf{C}}(E - E_{0C})/hN_{\mathbf{2}}(E)]$$

with $\sum P^{\ddagger}_{\mathbf{2D}}(E - E_{0D})$ and $\sum P^{\ddagger}_{\mathbf{C}}(E - E_{0C})$ being the sum of states of the transition structures for dissociation of complex $\mathbf{2C_2}$ into protonated oxetane plus water (**2D**) and for isomerization $\mathbf{2H_a}^+ \Leftrightarrow \mathbf{2C_2}$ (**2TS−C**). As long as E refers to the ground state of $\mathbf{2H_a}^+$, the critical energies values used in the calculation are $E_{0D} = 144$ kJ/mol (1.49 eV) and $E_{0C} = 137$ kJ/mol (1.42 eV). The two representative curves $k_{2a}(E)$ and $k_{2b}(E)$ in the range of internal energy $E = 1-5$ eV are presented in Figure 8.

The most obvious conclusion which may be drawn from the data presented in Figure 8 is that the cyclodehydration reaction a occurs at a slower rate at high energy E than the concerted

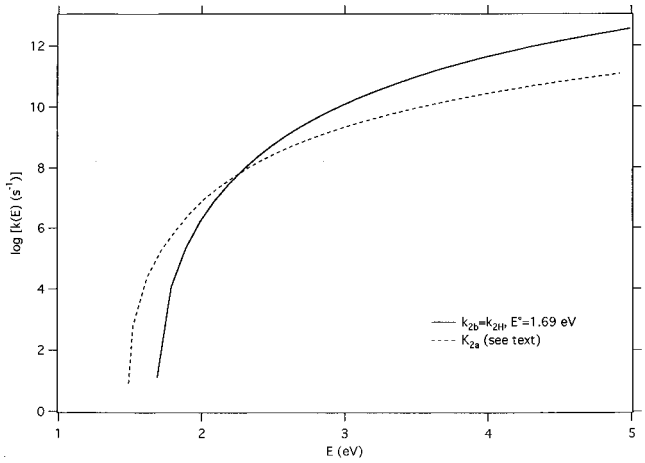

Figure 8. RRKM rate constants for the cyclodehydration (k_{2a}) and the dehydration assisted by a 1,3-hydride ion transfer (k_{2b}) from protonated 1,3-propanediol (see text for the full meaning of each rate constant).

1,3-hydride ion shift/dehydration process b. At 5 eV k_{2a} is lower than k_{2b} by more than one order of magnitude. The intercept of the two curves arises for an internal energy E of ca. 2.25 eV and the corresponding rate constant's value is 5×10^7 s^{-1}, i.e. a value greater than the rate constant of $\approx 10^5$ s^{-1} allowed for metastable dissociations. Thus most of the dissociations of ions $\mathbf{2H}^+$ occurring in the ion source of the mass spectrometer, i.e. with a rate constant greater than $\approx 10^6$ s^{-1}, proceed via the path b to give protonated propanal.

Considering now the dissociation of metastable ions $\mathbf{2H}^+$ for which the rate constant is close to 10^5 s^{-1}, the favored process is clearly reaction a. The corresponding internal energy, determined from the equality $k_{2a} = 10^5$ s^{-1}, is E* = 1.70 eV. At this energy k_{2b} is close to 10 s^{-1}, and the reaction b cannot compete with process a.

In summary, the experimental results concerning the dehydration of protonated 1,3-propanediol may be accounted for by the simple model of competitive reactions a and b presented in Scheme 4. Only the former process arises from metastable ions $\mathbf{2H}^+$, the latter being increasingly important as the internal energy increases to becomes dominant for most of the dissociations occurring in the ion source.

Protonated 1,4-Butanediol, $\mathbf{3H}^+$. The methane chemical ionization mass spectrum of 1,4-butanediol, **3**, presents an intense peak corresponding to the water loss $[\mathbf{3H}-H_2O]^+$ (53% of the base peak $\mathbf{3H}^+$).[1c] Unimolecular decompositions of metastable $\mathbf{3H}^+$ ions lead exclusively to $[\mathbf{3H}-H_2O]^+$ ions, a reaction involving only the protonating and the hydroxylic hydrogens. The metastable peak is simple Gaussian, and thus only one reaction mechanism seems to be operative at least at low internal energy. The corresponding kinetic energy releases are $T_{0.5} = 28 \pm 3$ meV and $T_{average} = 76 \pm 7$ meV.

The characterization of $[C_4H_9O]^+$ ions by CA mass spectrometry has been explored some years ago.[18] Results obtained using the six-sectors mass spectrometer are reported in Table 6.

A clear distinction between protonated butanal and protonated tetrahydrofuran is afforded by the CA (He) and particularly, the CA (O_2) mass spectra. The former is characterized by an intense methane loss (*m/z* 57) and by a peak at *m/z* 35.5 (9%), corresponding to the formation of a doubly charged ion $[C_4H_7O]^{2+}$, while for protonated tetrahydrofuran a signal at *m/z* 42 is noticeable. The distribution of peak intensities *m/z* 27−31 may be also used to distinguish between the two structures. Finally, examination of Table 6 reveals a close analogy between the CA spectra of $[\mathbf{3H}-H_2O]^+$ and protonated tetrahydrofuran.

TABLE 6: CA (He) and CA (O_2) Spectra of *m/z* 73, $[C_4H_9O]^+$ Ions, Generated by Chemical Ionization from 1,4-Butanediol (3), Butanal (3a), and Tetrahydrofuran (3b)

		72	71	70	69	58	57	55	54	53	51	50	45	44	43	42	41	39	38	37	31	30	29	28	27	26
He	**3**	2	<1					205					1	32	100	35	18	23			54		12	4	30	
	3a	8	2			4	15	251		2	1	1	6	44	100	10	25	30			39		54	9	66	10
	3b	12	6	2	2		3	166		<1	<1	1	8	42	100	44	28	32			60		22	12	37	
O_2	**3**	7	11	2	2		5	409	3	5	3	3	6	63	100	69	40	45			50		22	9	28	10
	3a	10	2	1	1		60	400	7	8	3	3	6	93	100	21	33	38	12	7	32	6	52	15	47	16
	3b	10	9	2	1	1	4	383	3	5	3	3	6	58	100	65	38	42			50		23	10	29	11

TABLE 7: Total (hartree) and Relative (kJ mol^{-1}) Energies Calculated for the Protonated 1,4-Butanediol System

	HF/6-31G*			MP2(FC)/6-31G*//HF/6-31G*			MP2(FC)/6-311G**//HF/6-31G*		
species	total	rel	ZPE[a]	total	rel	+ZPE	total	rel	+ZPE
3H$^+$ (trans)	−307.305 19	94	392	−308.175 68	117	114			
3H$_a$ $^+$	−307.341 06	0	395	−308.220 40	0	0	−308.461 42	0	0
3C$_1$	−307.316 68	64	394	−308.188 66	83	82			
3TS−C	−307.310 44	80	386	−308.176 85	114	105	−308.416 25	119	110
3C$_2$	−307.334 53	17	389	−308.206 39	37	31			
[tetrahydrofuran]H$^+$	−231.307 99		330	−231.992 16			−232.160 32		
H_2O	−76.010 75		54	−76.195 96			−76.267 47		
[tetrahydrofuran]H$^+$ + H_2O	−307.318 74	59	384	−308.188 12	85	74	−308.427 79	88	77
3C$_3$	−307.354 80	−36	392	−308.230 90	−28	−31			
3TS−H	−307.264 13	202	374	−308.135 94	222	201			
[butanal]H$^+$	−231.302 23		319	−231.980 26			−232.151 96		
[butanal]H$^+$ + H_2O	−307.312 98	74	373	−308.176 22	116	94	−308.419 43	110	88
3C$_5$	−307.353 42	−32	381	−308.223 85	−9	−23			

[a] ZPE (corrected by the factor 0.9) in kJ mol^{-1}.

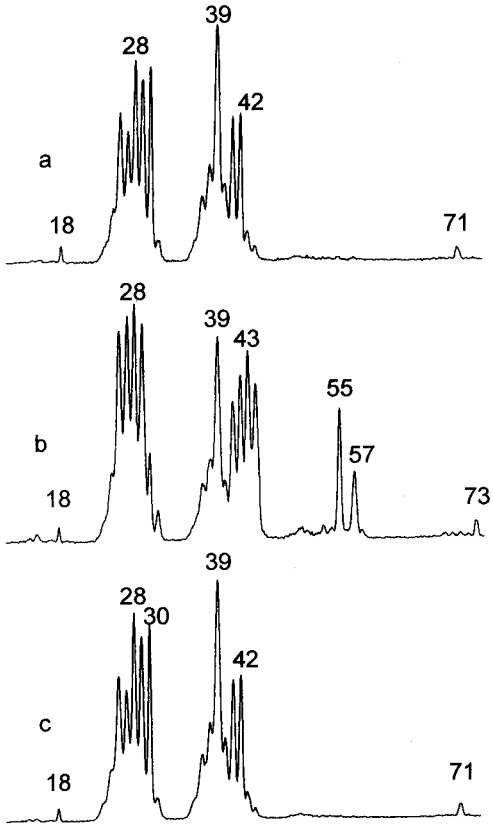

Figure 9. NR (NH_3/O_2) mass spectra of $[C_4H_9O]^+$ ions (*m/z* 73) produced from 1,4-butanediol (**3**) (a), butanal (**3a**) (b), and tetrahydrofurane (**3b**) (c).

The NR spectra fully confirm this conclusion (Figure 9): for both precursors, **3** and tetrahydrofuran, there is no recovered signal as expected for the corresponding hypervalent neutral which probably dissociates spontaneously to give a mixture of neutrals such as propene (*m/z* 42), formaldehyde (*m/z* 30), ethylene (*m/z* 28), etc. In contrast, neutralization/reionization of protonated butanal gives a small, but significant, recovered signal and peaks characteristic of the initial ionic structure

SCHEME 5

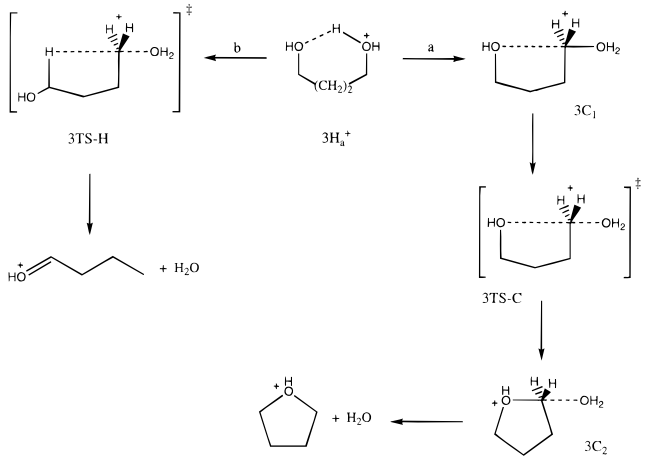

(particularly *m/z* 55 and 57). The noticeable signal at *m/z* 44 may be simply explained by the reionization of a molecule of vinyl alcohol produced by ethyl loss upon neutralization. These signals are completely absent from the NR spectrum of $[\mathbf{3H}-H_2O]^+$ ions. In conclusion, collisional experiments demonstrate unambiguously that only protonated tetrahydrofuran is produced by dehydration of protonated 1,4-butanediol in the source of the mass spectrometer. As long as this product is more stable than protonated butanal there is good chance that it is also produced at low internal energy; this point will be confirmed by the results of molecular orbital calculations.

The system **3H**$^+$ (Scheme 5) has been examined at the HF/6-31G* level during the geometry optimization procedure, and energies have been refined by inclusion of the electron correlation effect (MP2(FC)) and ZPE corrections with the 6-31G* basis set (Table 7). For the most significant points, calculations have been done at the MP2(FC)/6-311G**//HF/6-31G* level, but it is found that no appreciable change in relative energies is induced by the increase of the basis set size.

The 298 K relative energies of the products are calculated (MP2(FC)/6-31G*//HF/6-31G*) to be 79 and 102 kJ/mol for paths a and b, respectively, in reasonable agreement with

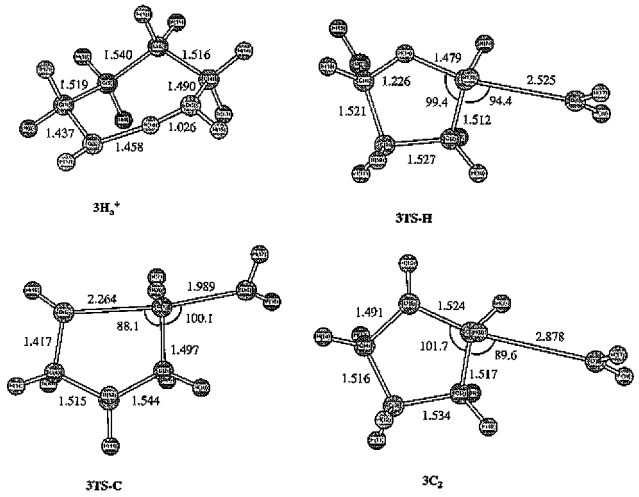

Figure 10. Geometrical parameters of some structures relevant to the protonated 1,4-butanediol system. Bond lengths are reported in angstroms and bond angles in degrees (HF/6-31G* optimized geometries).

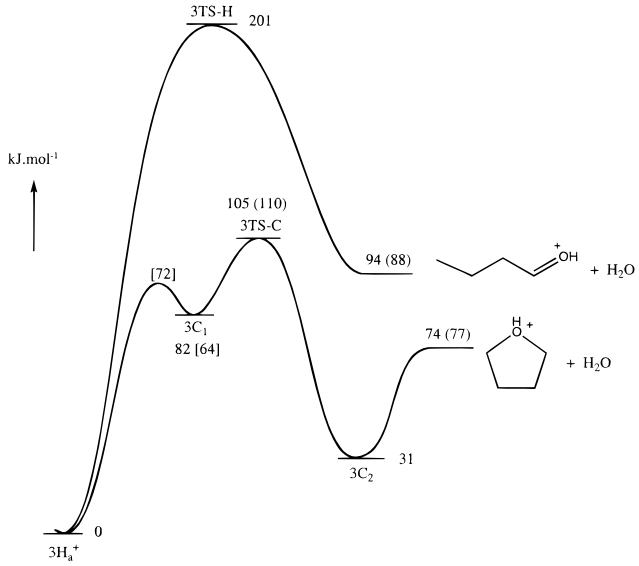

Figure 11. Schematic potential energy profile for dehydration reactions from the protonated 1,4-butanediol system (MP2/6-31G*//HF/6-31G*+ZPE, (in parentheses) MP2/6-311G**//HF/6-31G*, and (in brackets) HF/6-31G*//HF/6-31G* calculations).

experiment (75 and 88 kJ/mol, Table 1). The cyclized structure $\mathbf{3H_a}^+$ has been found to be the most stable conformation of protonated 1,4-butanediol (Figure 10), and it is more stable than the all-trans conformer $\mathbf{3H_b}^+$ by 114 kJ/mol. The internal hydrogen bond length is again shortened with respect to the lower homolog $\mathbf{2H}^+$ (1.458 Å for $\mathbf{3H_a}^+$ and 1.613 Å for $\mathbf{2H_a}^+$, geometries optimized at the HF/6-31G* level).

The cyclodehydration route (reaction a, Scheme 5) is also characterized by the formation of two intermediate ion-neutral complexes $\mathbf{3C_1}$ and $\mathbf{3C_2}$. The latter species is stabilized by 43 kJ/mol with respect to protonated tetrahydrofuran and water.

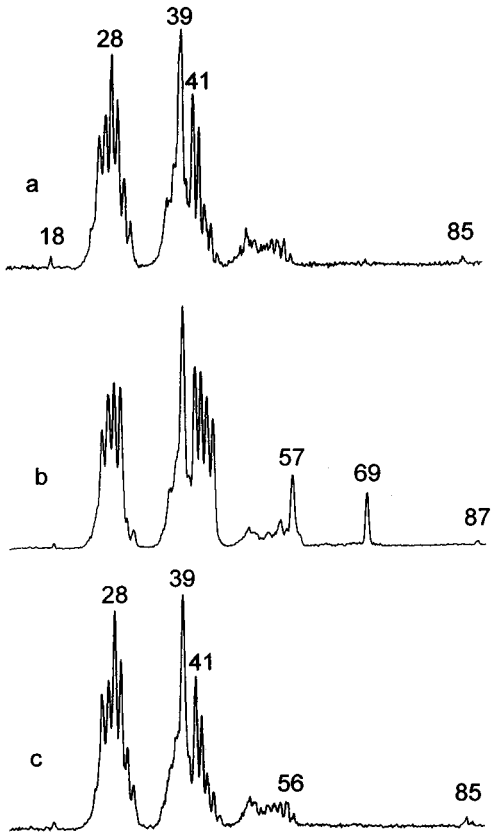

Figure 12. NR (NH_3/O_2) mass spectra of $[C_5H_{11}O]^+$ ions (*m/z* 87) produced from 1,5-pentanediol (**4**) (a), pentanal (**4a**) (b), and tetrahydropyrane (**4b**) (c).

The transition structure **3TS−C** is 105 kJ/mol above $\mathbf{3H_a}^+$ and, most importantly, 31 kJ/mol above the dissociation products, protonated tetrahydrofuran plus water. The complexes $\mathbf{3C_2}$ are thus generated, after passage through **3TS−C**, with a noticeable amount of vibrational energy and will spontaneously dissociate once produced.

The second dehydration reaction investigated involves a concerted 1,4-hydride ion migration (reaction b, Scheme 5). The transition structure **3TS−H** is found to lie 201 kJ/mol above $\mathbf{3H_a}^+$ and 107 kJ/mol above the products, protonated butanal plus water (Figure 11). An energy difference of no less than 96 kJ/mol separates the two transition structures **3TS−H** and **3TS−C**; there is consequently no doubt that the competition between these two reactions will be inefficient and that only reaction **a** should occur at low as well as at high internal energy. In conclusion, both calculation and experiment demonstrate the exclusive occurrence of the cyclodehydration reaction leading to protonated tetrahydrofuran from protonated 1,4-butanediol in the gas phase.

Protonated 1,5-Pentanediol, $\mathbf{4H}^+$. The dehydration reaction is the exclusive dissociation of metastable ions $\mathbf{4H}^+$, and it involves only the protonating and the hydroxylic hydrogens. The peak observed in the MIKE spectrum of $\mathbf{4H}^+$ is simple

TABLE 8: CA (He) and CA (O_2) Spectra of *m/z* 87, $[C_5H_{11}O]^+$ Ions, Generated by Chemical Ionization from 1,5-Pentanediol (4), Pentanal (4a), and Tetrahydropyran (4b)

		86	85	71	69	68	67	65	58	57	56	55	54	53	51	50	45	44	43	42	41	39	31	30	29	28	27	26
He	**4**				271	1				35	2	3		<1			5	1	6	2	100	25	24		12	3	15	
	4a	3			271				5	91		6		2			15	34	52	11	100	44	17		53	6	50	
	4b	6	<1		176	6				48	5	10	1	2			7	4	13	5	100	38	38		24	9	26	
O_2	**4**	7	4	4	628	35	20		6	49	15	20	11	13	5	5	25	20	22	17	100	43	28		29	16	25	
	4a	8		4	640		7		24	145		18		9	6	6	27	95	69	35	100	58	20	9	55	19	40	12
	4b	12	6	3	568	44	22	2	6	56	18	23	12	14	6	6	23	20	22	19	100	45	30		30	18	25	

TABLE 9: Total (hartree) and Relative (kJ mol^{-1}) Energies Calculated for the Protonated 1,5-Pentanediol System

	HF/3-21G		HF/6-31G*			MP2(FC)/6-31G*//HF/6-31G*		
species	total	rel	total	rel	ZPE[a]	total	rel	+ZPE
4H$^+$ (trans)			−346.341 27	86	465	−347.342 63	110	107
4H$_a$ $^+$	−344.506 02	0	−346.374 23	0	468	−347.384 56	0	0
4C$_1$	−344.464 09	110	−346.350 81	62	467	−347.354 36	79	78
4TS−C	−344.458 30	125	−346.343 62	80	458	−347.340 11	117	107
4C$_2$	−344.485 71	53	−346.375 36	3	464	−347.379 22	14	10
[tetrahydropyran]H$^+$	−268.876 63		−270.349 61		405	−271.165 86		
H_2O	−75.585 96		−76.010 75		54	−76.195 96		
[tetrahydropyran]H$^+$ + H_2O	−344.462 59	114	−346.360 36	36	459	−347.361 82	60	51
4C$_3$	−344.520 82	−39	−346.396 10	−57	466	−347.404 17	−51	−53
4TS−H	−344.404 00	268	−346.312 30	163	448	−347.314 22	185	165
[pentanal]H$^+$	−268.834 20		−270.337 94		391	−271.146 86		
[pentanal]H$^+$ + H_2O	−344.420 16	225	−346.348 69	67	446	−347.342 82	110	88
4C$_5$	−344.487 76	48	−346.388 92	−39	454	−347.390 18	−15	−29

[a] ZPE (corrected by the factor 0.9) in kJ mol^{-1}.

SCHEME 6

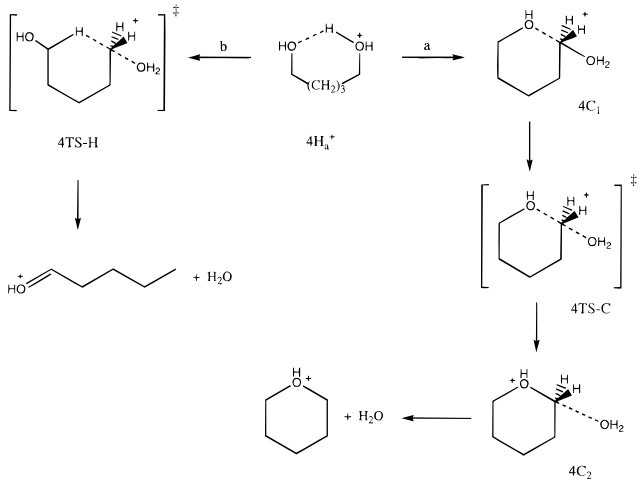

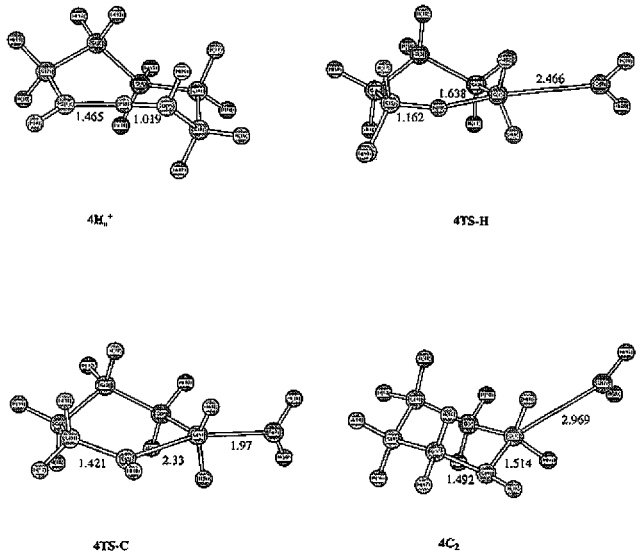

Figure 13. Geometrical parameters of some structures relevant to the protonated 1,5-pentanediol system. Bond lengths are reported in angstroms and bond angles in degrees (HF/6-31G* optimized geometries).

Gaussian with the following characteristics: $T_{0.5} = 31 \pm 3$ meV and $T_{average} = 76 \pm 7$ meV.

Concerning the $[C_5H_{11}O]^+$ fragment ions, the two potential candidates, protonated pentanal and protonated tetrahydropyran, may be easily characterized by their CA spectra. Distinct differences may be observed in the *m/z* 27−31, 39−45, and 53−57 regions in the CA (He) and, particularly, in the CA (O_2) spectra (Table 8).

The spectrum of [**4H**−H_2O]$^+$ fragment ions agrees with the formation of protonated tetrahydropyran by dehydration of **4H**$^+$ in the source of the mass spectrometer. This conclusion is also supported by the NR spectra which are identical for 1,5-pentanediol and tetrahydropyran precursors but different from that of protonated pentanal (Figure 12). In the former cases, no recovered signal is detected in accordance with the formation of an unstable hypervalent neutral. For protonated pentanal, a weak recovered signal is observed together with peaks at *m/z* 69 and 57, corresponding to water and ethane losses, respectively (the last reaction is analogous to the methane loss observed in the NR spectrum of protonated butanal).

Molecular orbital calculations have been done at the MP2/6-31G*//HF/6-31G*+ZPE level. The two reaction mechanisms presented in Scheme 6 have been studied.

The results are presented in Table 9 and in Figure 13. Calculation of the 298 K heat of reaction a and b leads to $\Delta_a H°_{298} = 54$ kJ/mol and $\Delta_b H°_{298} = 95$ kJ/mol, a set of results comparable to the experimentaly based values of 73 and 100 kJ/mol presented in Table 1. The most stable structure of protonated 1,5-pentanal is the conformer **4H$_a$**$^+$ which presents an internal hydrogen bond. The hydrogen bond length is calculated to be equal to 1.465 Å at the HF/6-31G* level of geometry optimization; at this same level the H-bond length in **1H$_a$**$^+$, **2H$_a$**$^+$, and **3H$_a$**$^+$ were 1.889, 1.613, and 1.458 Å,

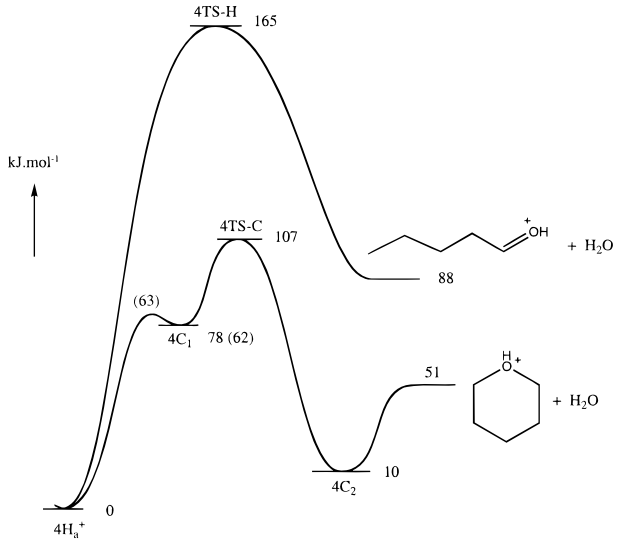

Figure 14. Schematic potential energy profile for dehydration reactions from the protonated 1,5-pentanediol system (MP2/6-31G*//HF/6-31G* + ZPE and (in parentheses) HF/6-31G*//HF/6-31G* calculations).

respectively, in agreement with the expected decrease of strain energy. The all-trans structure $\mathbf{4H_b}^+$ is less stable than $\mathbf{4H_a}^+$ by 107 kJ/mol at the MP2(FC)/6-31G*//HF/6-31G*+ZPE level. Qualitatively, the present data compare well with the previous system: the cyclodehydration route (reaction a, Scheme 6) is largely favored over the hydride ion migration (reaction **b**, Scheme 6) as illustrated by the schematic potential energy profile presented in Figure 14. The two corresponding transition structures are situated 107 and 165 kJ/mol, respectively, above the most stable structure $\mathbf{4H_a}^+$. Again, two stable complexes $\mathbf{4C_1}$ and $\mathbf{4C_2}$ are formed during the cyclodehydration reaction. It must be noted however that $\mathbf{4C_1}$ lies in a very shallow well. The stabilization energy of $\mathbf{4C_2}$ with respect to protonated tetrahydropyran and water is equal to 41 kJ/mol. The transition structure **4TS−C** is 56 kJ/mol above the cyclodehydration products; consequently, as also observed for 1,4-butanediol, the complexes $\mathbf{4C_2}$ produced from $\mathbf{4H_a}^+$ are highly vibrationally excited species and rapidly dissociate into protonated tetrahydropyran plus water.

The difference in energy between the transition structures **4TS−H** and **4TS−C**, 58 kJ/mol, renders the observation of a competition between the two reactions impossible. Only the formation of protonated tetrahydropyran is kinetically allowed. This confirms the conclusion based on experiment that only the cyclodehydration reaction producing protonated tetrahydropyran is occurring from protonated 1,5-pentanediol in the gas phase.

Conclusion

The lowest energy dissociation process of protonated α,ω-diols in the gas phase is the dehydration reaction. The present experimental and theoretical study reveals the following findings:

(1) Two reaction mechanisms were found to satisfactorily explain the experimental observations. One leads to a protonated cyclic ether via an internal nucleophilic substitution and one gives a protonated carbonyl species after hydride ion transfer from the α-carbon to the ω-position.

(2) The dehydration of protonated 1,2-ethanediol occurs via the classic pinacol rearrangement, and the critical energy for this concerted 1,2-hydride shift/water loss process is calculated (MP2/6-311G**//MP2/6-31G*+ZPE level) to be 99 kJ/mol.

(3) For 1,3-, 1,4-, and 1,5-diols the dehydration reaction produces the corresponding protonated cyclic ether after isomerization into a very stable electrostatic complex between the two dissociation products. The energy-determining step is the dissociation of the complex in the case of 1,3-propanediol and its formation (the cyclization step) in the case of 1,4-butanediol and 1,5-pentanediol. Calculated critical energies are 144, 110 and 107 kJ/mol, respectively.

(4) A parallel formation of protonated propanal is observed beside protonated oxetane from protonated 1,3-propanediol at high internal energy. The calculated critical energy for this reaction is equal to 163 kJ/mol. This competition is explained in terms of the internal energy effect upon the two competitive rate constants.

The contrasted behavior of the four members of the studied α,ω-diols series appears to be due to the combined effects of the order of stability of the dissociation products along the series, and the non-negligible critical energies associated to both dehydration channels.

Acknowledgment. The authors thank the Institut du Developpement et des Ressources en Informatique Scientifique, IDRIS (Orsay), for providing computational time (Grant 960784) and the Fonds National de la Recherche Scientifique for its contribution to the purchase of the large scale Micromass-AutoSpec-6F mass spectrometer.

References and Notes

(1) (a) Splitter, J. S.; Turecek, F. *Applications of Mass Spectrometry to Organic Stereochemistry*; VCH Publishers, Inc.: New York, 1994. (b) Eichmann, E. S.; Alvarez, E.; Brodbelt, J. S. *J. Am. Soc. Mass Spectrom.* **1992**, *3*, 535. (c) Chen, Q. F.; Stone, J. A. *J. Phys. Chem.* **1995**, *99*, 1442. (d) Ashkenazi, P.; Domon, B.; Gutman, A. L.; Mandelbaum, A.; Mueller, D.; Richter, W. J.; Ginsburg, D. *Isr. J. Chem.* **1989**, *29*, 131.

(2) (a) Bartok, M.; Molnar, A. *Chemistry of Ethers, Crown Ethers, Hydroxyl Groups Their Sulphur Analogues*; Pataï, S., Ed.; Wiley: Chichester, U.K., 1980; Vol. 2, pp 721−60. (b) Diab, J.; Abou-Assali, M.; Gervais, C.; Anker, D. *Tetrahedron Lett.* **1985**, *26*, 1501. (c) Kotkar, D.; Ghosh, P. K. *J. Chem. Soc., Chem. Commun.* **1986**, 650. (d) Bezouhanova, C. P.; Jabur, F. A. *React. Kinet. Catal. Lett.* **1993**, *51*, 177. (e) Wali, A.; Ganeshpure, P. A.; Muthukumaru Pillai, S.; Satish, S. *Ind. Eng. Chem. Res.* **1994**, *33*, 444.

(3) (a) Lias, S. G.; Bartmess, J. E.; Liebman, J. F.; Holmes, J. L.; Levin, R. D.; Mallard, W. G. Gas Phase Ion and Neutral Thermochemistry. *J. Phys. Chem. Ref. Data* **1988**, *17*, Suppl. 1. (b) Szulejko, J. E.; McMahon, T. B. *J. Am. Chem. Soc.* **1993**, *115*, 7839.

(4) (a) Wesdemiotis, C.; McLafferty, F. W. *Chem. Rev.* **1987**, *87*, 485. (b) Terlouw, J. K.; Schwarz, H. *Angew. Chem., Int. Ed. Engl.* **1987**, *26*, 805. (c) Holmes, J. L. *Mass Spectrom. Rev.* **1989**, *8*, 513. (d) McLafferty, F. W. *Science* **1990**, *247*, 925. (e) Goldberg, N.; Schwarz, H. *Acc. Chem. Res.* **1994**, *27*, 347. (f) Flammang, R.; Gallez, L.; Van Haverbeke, Y.; Wong, M. W.; Wentrup, C. *Rapid Commun. Mass Spectrom.* **1996**, *10*, 232.

(5) Holmes, J. L.; Osborne, A. D. *Int. J. Mass Spectrom. Ion Processes* **1977**, *23*, 189.

(6) Bateman, R. H.; Brown, J.; Lefevere, M.; Flammang, R.; Van Haverbeke, Y. *Int. J. Mass Spectrom. Ion Processes* **1992**, *115*, 205.

(7) Frisch, M. J.; Trucks, G. W.; Schlegel, H. B.; Gill, P. M. W.; Johnson, B. G.; Robb, M. A.; Cheesemann, J. R.; Keith, T. A.; Petersson, G. A.; Montgomery, J. A.; Raghavachari, K.; Al-Laham, M. A.; Zakrewski, V. G.; Ortiz, J. V.; Foresman, J. B.; Cioslowski, J.; Stefanov, B. B.; Nanayakkara, A.; Challacombe, M.; Peng, C. Y.; Ayala, P. Y.; Chen, W.; Wong, M. W.; Andres, J. L.; Replogle, E. S.; Gomperts, R.; Martin, R. L.; Fox, D. J.; Binkley, J. S.; Defrees, D. J.; Baker, J.; Stewart, J. P.; Head-Gordon, M.; Gonzales, C.; Pople, J. A. *Gaussian 94 Revision*, Gaussian, Inc., Pittsburgh, PA, **1995**.

(8) (a) McLafferty, F. W.; Kornfeld, R.; Haddon, W. F.; Levsen, K.; Sakai, I.; Bente, P. F., III; Tsai S.-C.; Schuddemage H. D. R. *J. Am. Chem. Soc.* **1973**, *95*, 3886. (b) Van de Graaf, B.; Dymerski, P. P.; McLafferty, F. W. *J. Chem. Soc., Chem. Commun.* **1975**, 978. (c) Burgers, P. C.; Terlouw, J. K.; Holmes, J. L. *Org. Mass Spectrom.* **1982**, *17*, 369. (d) Polce, M. J.; Cordero, M. M.; Wesdemiotis, C.; Bott, P. A. *Int. J. Mass Spectrom. Ion Processes* **1992**, *113*, 35.

(9) Bouchoux, G.; Jezequel, S.; Penaud-Berruyer, F. *Org. Mass Spectrom.* **1993**, *28*, 421.

(10) Ford, G. P.; Smith, C. T. *J. Am. Chem. Soc.* **1987**, *109*, 1325.

(11) Nakamura, K.; Osamura, Y. *J. Phys. Org. Chem.* **1990**, *3*, 737.

(12) (a) Nobes, H. R.; Rodwell, W. R.; Bouma, W. J.; Radom, L. *J. Am. Chem. Soc.* **1981**, *103*, 1913. (b) Bock, C. W.; George, P.; Glusker, J. P. *J. Org. Chem.* **1993**, *58*, 5816. (c) Curtiss, L. A.; Lucas, D. J.; Pople, J. A. *J. Chem. Phys.* **1995**, *102*, 3292.

(13) Forst, W. *Theory of Unimolecular Reactions*; Academic Press: New York, 1973.

(14) Stein, S. E.; Rabinovitch, B. S. *J. Chem. Phys.* **1973**, *58*, 2438.

(15) (a) Klots, C. E. *J. Chem. Phys.* **1973**, *58*, 5364. (b) Baer, T. *Adv. Chem. Phys.* **1986**, *64*, 111.

(16) (a) McLafferty, F. W.; Sakai, I. *Org. Mass Spectrom.* **1973**, *7*, 971. (b) Harrison, A. G.; Gaumann, T.; Stahl, D. *Org. Mass Spectrom.* **1983**, *18*, 517.

(17) Lin, P.; Kenttämaa, H. I. *J. Phys. Org. Chem.* **1992**, *5*, 201.

(18) Maquestiau, A.; Beugnies, D.; Flammang, R.; Houriet, R.; Bouchoux, G. *Rapid Commun. Mass Spectrom.* **1988**, *2*, 176.

(19) Baer, T.; Brand, W. A.; Bunn, T. L.; Butler, J. *J. Faraday Discuss. Chem. Soc.* **1983**, *75*, 45, see also: (a) Miller, A. R. *J. Chem. Phys.* **1976**, *65*, 2216. (b) Chesnavich, W. J.; Bowers, M. T. *J. Am. Chem. Soc.* **1977**, *99*, 1705.